In-plane magnetocrystalline anisotropy observed on Fe/Cu(111) nanostructures grown on stepped surfaces

C. Boeglin,[1,*] S. Stanescu,[1] J. P. Deville,[1] P. Ohresser,[2] and N. B. Brookes[3]
[1]*IPCMS-GSI-UMR 7504, F-67037 Strasbourg Cedex, France*
[2]*LURE, F-91405 Orsay, France*
[3]*ESRF, BP 220, F-38043 Grenoble Cedex, France*
(Received 21 February 2002; published 19 July 2002)

Magnetic in-plane and out-of-plane anisotropies measured by angle dependent x-ray magnetic circular dichroism (XMCD) on fcc Fe nanostructures are discussed and compared with fcc FeNi nanostructures. All studies were performed using XMCD at the Fe $L_{2,3}$ edges for Fe grown on a Cu(111) vicinal vic surface. The step induced in-plane anisotropy in the step decoration regime is analyzed by measuring the orbital magnetic moment dependence as a function of the in-plane azimuth and out-of-plane incidence angles. In the one-dimensional limit where the out-of-plane magnetic easy axis dominates, Fe/Cu(111) shows a large in-plane orbital magnetic moment anisotropy leading to a magnetocrystalline anisotropy energy of 0.4 meV/atom and an in-plane magnetic easy axis perpendicular to the steps. In the nanometer scale the aspect ratio of the elongated rectangular Fe stripes are found to be responsible for the in-plane and out-of-plane anisotropy. This is coherent with previous findings where the circular shaped fcc $Fe_{0.65}Ni_{0.35}$ nanostructures do not show any in-plane anisotropy. The three-dimensional nanostructures are characterized by magnetic orbital moments connected with the number of broken bonds in the direction of the quantization axis defined by the direction of the saturation field. The microscopic origin of the in-plane large orbital magnetic moment anisotropy is attributed to the nanometer size of the structures perpendicular to the steps and to the asymmetry of the number of broken bonds in the plane.

DOI: 10.1103/PhysRevB.66.014439 PACS number(s): 75.70.Cn, 75.70.Ak, 78.70.Dm

I. INTRODUCTION

Magnetic nanostructures are nowadays among the most interesting subjects where the microscopic structures and the magnetic anisotropy are ultimately related. Reduced symmetry and cluster size effects of ferromagnetic nanostructures are challenging tasks for both experimentalists and theoreticians. In particular, ultrathin films can exhibit strong out-of-plane anisotropy. For thin films the magnetocrystalline anisotropies (favoring out-of-plane magnetization) and the magnetostatic anisotropy (favoring the in-plane one) are the mean contributions to the total macroscopic magnetic anisotropy. Strain relaxation in thin epitaxial films generally favors magnetocrystalline anisotropy whereas the bulk contribution favors the magnetostatic anisotropy. More recently our interest was focused on reduced one-dimensional (1D) symmetry systems where oriented nanostructures lead to out-of-plane and in-plane magnetic anisotropies. In this framework it is of interest to look for the microscopic origin of 1D stripe anisotropies (in the plane and out of the plane). These anisotropies are known to be related either to strain relaxation (tetragonalisation) of the structures or to a large number of broken bonds in one direction. Surfaces (or interfaces) are known to be at the origin of the perpendicular magnetic anisotropy. We should thus be able to generalize this argument to the in-plane geometry.

Many self-organized systems have been studied recently (Co/Cu(100), Fe/Cu(111), $Fe_{65}Ni_{35}$/Cu(111), Co/Au(111), $\cdots$) in order to correlate the reduced dimensionality of clusters and surfaces to the increased magnetic moments.[1–5] The mean results show that the magnetic orbital moments are strongly increased when reducing the size of the nanostructures. This is explained by considering the contribution from the edge and surface atoms where the quenching of the orbital magnetic moment is less effective than that of the bulk.

But for most of these systems, the strain and the broken bond effects are almost indistinguishable because the films show both effects simultaneously in a given growth regime. Our aim is to separate the regime where no strain relaxation occurs in order to relate the anisotropies of the nanostructures to the broken bonds and aspect ratio of the structures. This is the case for stripes in Fe/Cu(111) grown at room temperature on vicinal surfaces and below the 2D coalescence. We will show that the magnetocrystalline anisotropy measured on Fe/Cu(111) nanostructures can be attributed to the effect of the anisotropy of the number of broken bonds and the associated electronic structure. At a given temperature the anisotropy of these materials are given in a simplified approach by a constant volume and a $1/d$ (where d is the thickness of the film) surface-dependent term. A generalization of this concept along any direction is thought to be possible inside the plane when specific structural or configuration anisotropies are present. For instance, this is the case by growing self-similar magnetic nanostructures through diffusion on controlled surface defects such as regular steps on vicinal surfaces.

Magneto-optic Kerr experiments performed on thin ferromagnetic layers [Fe/W(001), Co/Cu(100), Fe/Ag(100)][6–11] deposited on vicinal surfaces show the existence of step induced uniaxial anisotropies. Depending on the thin ferromagnetic layers, the growth mode and the step density[12] the in-plane orientation of the easy axis remains parallel or perpendicular to the steps irrespectively to the crystallographic

orientation. The important remaining question is to know what is responsible for the either parallel or perpendicular orientation of the magnetic easy axis for these systems. In this framework, recent self-consistent tight-binding MAE calculations from J. Dorantes-Davila[13] show that for $3d$ metals the easy axis of magnetization for 1D chains and 2D ladders is oriented either out of plane, in-plane parallel or in-plane perpendicular to the chains, depending on the electronic configuration. For example, Fe infinite monatomic chains show a parallel in-plane easy axis of magnetization whereas multichains with interchain packing of triangular symmetry show a perpendicular easy axis of magnetization, demonstrating the crucial role of the structure in the low-dimensional systems.

At present, the element specific orbital (M_L) and spin (M_S) magnetic moments can be derived by x-ray magnetic circular dichroism (XMCD) applying the sum rules. The high sensibility of the XMCD technique has favored recently many experimental works in the nanostructured 0.01-monolayer (ML)–1-ML range. In the absence of alloying the magnetic moment M_S relates generally to the atomic volume of the element and M_L to the electronic structure influenced by the hybridization and strain in the film. Conversely, the magnetic orbital moment anisotropies are far less understood in this thickness range. Besides the effect of the electronic hybridization at the interfaces and of tetragonalization in the strain relaxation regime, in the very low thickness range (0–0.8 ML) the microscopic origin of the strong orbital moment anisotropy is still an open question. The strong electron localization caused by low atomic coordination occurring for the low-dimension nanostructures is thought to be the main origin of the strong orbital moments and anisotropies. Nevertheless, for most of the experimentally grown thin films, the two parameters (structure and reduced symmetry) are often superimposed so that no simple relationship can be drawn between one and the other microscopic phenomena and the observed moments. Using well characterized Fe nanostructures grown on a Cu(111) vicinal surface[14,15] in the pseudomorphic (Fe fcc) thickness range we have the possibility to measure along the 3D coordinates all the magnetic parameters and to compare them to the density of broken bonds.

Thus in the absence of tetragonalization (before the relaxation of the epitaxial strain) the M_L anisotropy can be shown to be configurational in origin. Epitaxial nanostructures grown by self-diffusion on patterned substrates can thus show specific directions along which reduced coordinations are found and thus lead to a direction dependent orbital moment which provides the macroscopic magnetic anisotropy. We will show that this is the case for elongated Fe stripes grown along the step edges of vicinal surfaces where a reduced number of nearest neighbors (NN's) is obtained along the perpendicular to the step direction whereas parallel to the steps large NN numbers are found. We will also show that the reduced number of NN's along the growth direction leads to large out-of-plane anisotropies of the orbital magnetic moment. These anisotropies are coherent with those measured in the plane considering the number of NN's. The local electronic structures associated with the number of broken bonds are directionally dependent and related to the directional dependence of M_L.

In Sec. II we shall describe the angle-dependent MCXD results obtained at the Fe $L_{2,3}$ edges and we shall discuss the results with respect to the growth mode and morphology of Fe in the submonolayer regime on vicinal Cu(111) surface. Finally in Sec. III we shall discuss the origin of the measured orbital magnetic moment anisotropies.

II. EXPERIMENT

A. Experimental setup

The structural studies have been carried out in a UHV system with a base pressure of 1×10^{-10} mbar equipped with Auger electron spectroscopy (AES), low-energy electron diffraction (LEED) and scanning tunneling microscopy (STM). The substrate, further labeled as Cu(111)-vic, is cut from a Cu(111) single crystal at 1.2° from the $[111]$ direction. The monoatomic steps are parallel to the $[1\bar{1}0]$ direction and perpendicular to the $[\bar{1}\bar{1}2]$ one, leading to (111) microfacets. The substrates were cleaned by repeated cycles of Ar^+ sputtering and annealing at 850 K. After elimination of all impurities, checked by AES, it was verified by STM that straight and parallel steps with an average terrace length of 9 nm for the 1.2° miscut sample were obtained. In agreement with previous studies on Fe/Cu(111)-vic 1.2° (Ref. 14) $a\ p(1\times1)$ LEED pattern with a threefold symmetry was observed up to 2-ML Fe deposition indicating a pseudomorphic growth of the Fe fcc film.

For the XMCD experiments the Cu(111) single-crystal substrates were prepared under ultrahigh vacuum conditions (1×10^{-10} mbar). During these experiments the thickness of the thin film was checked by measuring the x-ray-absorption Fe L_3 edge heights as previously reported for $Fe_{65}Ni_{35}$ ultrathin films.[3] The XMCD experiments were performed at the ID12B beamline of the European Synchrotron Radiation Facility in Grenoble by monitoring the total electron yield. The XMCD measurements were performed at saturation for different incidence and azimuthal angles of the light, applying the magnetic field parallel to the incident circular polarized light. The XMCD spectra were obtained by reversing both the magnetic field (±4 T) and the helicity of the light at 10 K. In order to check and insure the magnetic saturation along the quantization axis we record the XMCD magnetization cycles at the Fe L_3 edge.

B. XMCD measurements

X-ray magnetic circular dichroism in the $L_{2,3}$ absorption edges gives access to an element specific local magnetic moment. A theoretical analysis performed in an atomic framework predicts that for $2p$-$3d$ transitions the ground-state expectation values for the spin and orbital magnetic moments can be derived.[16,17] In this paper we will use these sum rules to extract the values of the orbital magnetic moment M_L and the effective spin magnetic moment M_S^{eff} per hole. A constant hole number of 3.34 per iron atom has been introduced and does not affect any relative variation of M_L or M_S^{eff}. This

point is supported by Stöhr[18] showing that reduced symmetry does not change significantly the electron or hole distribution. This allows to compare our M_L and M_S^{eff} values with that of bcc iron grown after 2.5-ML Fe/Cu(111)-vic. We can neglect the saturation effects in total electron yield at the Fe $L_{2,3}$ edges because the thickness of our films does not exceed 8 Å which is small compared to the escape depth (17 Å) and to the x-ray penetration at 710 eV.[19] Assuming this limited thickness of the films the orbital moment and the effective spin magnetic moment can be measured as a function of the film thickness. Moreover, in the case of the nanostructures studied in this work, the incidence angle dependence of the XMCD signal is affected by errors less than 5% due to saturation effects in total yield measurements.[20] The azimuth variations of the in-plane spin and orbital magnetic moments are insensitive to such effects.

The Fe $L_{2,3}$ XMCD spectra, recorded in the total yield detection mode were performed using a 7-T cryomagnet. The sample holder allowed polar (θ) and azimuthal rotations (φ) of the sample around the surface normal as already described by Cherifi *et al.*[3] The incidence angle (θ) dependence of the XMCD signal was measured along different azimuthal angles defined by the direction of the steps. These measurements where performed in order to extract the out-of-plane magnetic anisotropies relative to the in-plane step directions and the in-plane magnetic anisotropies. The magnetization direction could thus be tuned between parallel ($\varphi=0°$) and perpendicular ($\varphi=90°$) to the steps at a constant incidence angle θ. The incident x-ray beam is 90% circularly polarized and is kept parallel to the saturated magnetization direction during the XMCD measurements. In Fig. 1 we present a pair of typical normalized x-ray-absorption spectra at the Fe $L_{2,3}$ edges for 0.15-ML Fe/Cu(111)-vic 1.2° obtained by reversing the magnetic field from the parallel to the antiparallel alignment in respect to the photon spin. Below we show two XMCD differences and the related integrated spectra obtained for two different geometries in respect to the steps. The magnetic moments M_L and M_S^{eff} are extracted from the XMCD spectra using the sum rules[16,17] where for the $L_{2,3}$ edges one has

$$M_L = -\frac{4qN_h}{3R_{\text{iso}}}, \tag{1}$$

$$M_S^{\text{eff}} = M_S + M_T(\theta) = -\frac{(6p-4q)N_h}{R_{\text{iso}}}, \tag{2}$$

where p and q are, respectively, the integrals over L_3 and L_2+L_3 of the XMCD difference and R_{iso} is the integrated isotropic spectrum assumed to be equal to the magnetization-averaged absorption cross section. N_h is the number of holes in the $3d$ electronic states. M_T (θ) is the dipolar spin moment, generally neglected for $3d$ metals.

Between the direction parallel to the steps ($\varphi=0°$) and perpendicular to the steps ($\varphi=90°$) the Fe $L_{2,3}$ integrated value q doubles and can be correlated with the in-plane orbital magnetic moment anisotropy. For each azimuth a complete set of values of M_L (θ) and M_S (θ) is measured between $0<\theta<50°$ in order to extract the out-of-plane anisotropy of the magnetic moments.

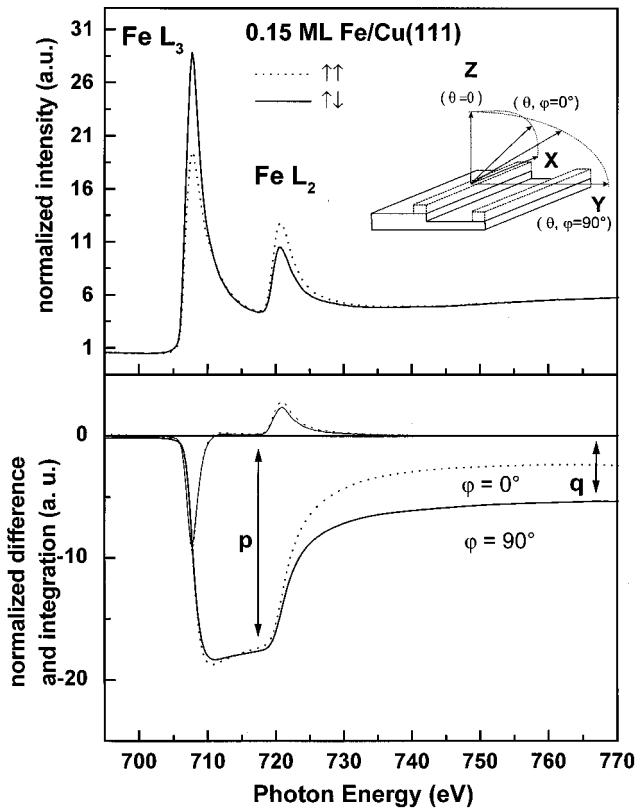

FIG. 1. Two XMCD spectra at the Fe $L_{2,3}$ edges obtained for 0.15 ML at $\theta=50°$ for the parallel and the antiparallel alignment between the incident light and the applied magnetic field. The normalized differences of the XMCD spectra are presented at the bottom and we compare the results obtained parallel to the steps and perpendicular to the steps ($\varphi=0°$ and $\varphi=90°$, respectively). The difference is noticeable at the L_2 edge. The integration over the Fe $L_{2,3}$ is plotted in order to evidence the large orbital magnetic moment difference (proportional to q) between the two geometries. In the inset we present the XMCD geometry defining the incidence angle θ and the azimuth φ with respect to the iron stripes.

In Fig. 2 we show the evolution of the three components of the orbital magnetic moments M_L^Z, M_L^X M_L^Y with the Fe film thickness. These components are extracted applying the sum rules and the $\sin^2(\theta)$ dependence of the orbital moment anisotropy[21,22] along the specific azimuths in order to extract the projected in-plane components (M_L^X and M_L^Y). For example, one can extract the in-plane M_L^X component following the expression

$$M_L(\theta,\ \varphi=0) = M_L^X + [M_L^X - M_L^Z]\sin^2(\theta).$$

This will allow us to define the easy axis of magnetization if one assumes that for $3d$ metals it is related to the largest component of the orbital magnetic moment measured at saturation.[19–24] As will be discussed later, XMCD is restricted to the magnetocrystalline part of the magnetic anisotropy. Thus we will be able to define the easy axis of magne-

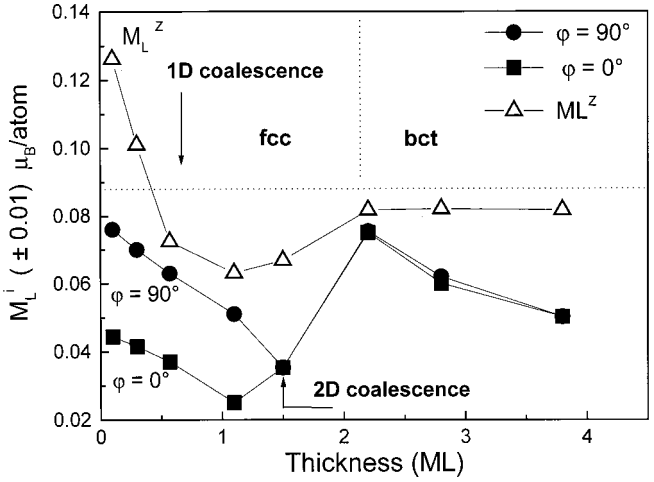

FIG. 2. Evolution of the magnetic orbital moment as a function of the thickness plotted for the *X*, *Y*, and *Z* direction. The open symbols are the out-of-plane M_L^Z magnetic orbital moments. The full symbols indicate the evolution of M_L^X and M_L^Y defined respectively by the two azimuths $\varphi=0°$ and $\varphi=90°$.

tization for the samples when the magnetocrystalline effect is dominant in the total macroscopic magnetic anisotropy.

The overall evolution observed in Fig. 2 corresponds to the results of Ohresser *et al.*[4] and shows that the moments are dependent on the fcc to bcc structural phase transition which occurs at 2.3-ML Fe/Cu(111)-vic 1.2°. If we compare the relative values of M_L^i $(i=x, y, z)$ along different directions of the Fe nanostructures we clearly find two thickness regimes. The first one is located before the 2D coalescence at 1.5-ML Fe where a splitting of all three components M_L^i is observed and the second one occurs after 1.5-ML Fe where both in-plane values of M_L^i are equivalent. Qualitatively, before 1.5 ML's the splitting of the values M_L^X, M_L^Y, and M_L^Z can be understood by the pseudomorphic fcc structure of iron on copper. In the absence of structural tetragonalization as reported by Shen *et al.*[15] the magnetocrystalline term reduces to the aspect ratio and broken bond effects of the Fe stripes. After the 2D coalescence a bct transformation of the structure leads to a Kurdjumov-Sachs (KS) superstructure. The structural phase transformation was shown to bring up a compression of the bcc structure in the *z* direction leading to a bct phase where the surface plane is (110) and defined by a threefold domain orientation.[15] This can be correlated to our XMCD data which show strongly enhanced magnetic orbital moments M_L^Z compared to the in-plane values M_L^X and M_L^Y. Moreover, due to the threefold symmetry of the KS domains in the plane of the 2D iron films neither the structure nor the morphology are expected to induce uniaxial anisotropies. We find by XMCD that no in-plane magnetic anisotropy is present at this stage of growth $(M_L^X=M_L^Y)$. The orbital magnetic moments measured by XMCD are restricted to the magnetocrystalline contribution of the magnetic anisotropy. The macroscopic measurements by magneto-optic Kerr effect[15] evidences the magnetic out-of-plane–in-plane transition of the easy magnetization axis at 2.3 ML's for Fe/Cu(111)-vicinal 1.2°. We thus show, comparing Kerr effect and XMCD data, that after the 2D coalescence and the fcc

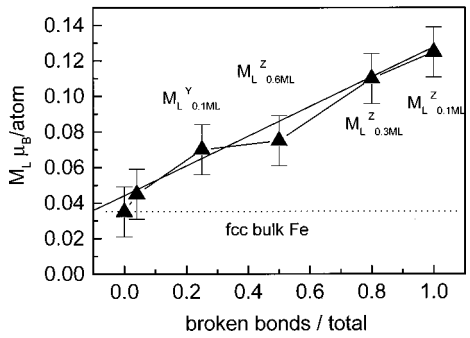

FIG. 3. Magnetic orbital moments M_L^i plotted as a function of the ratio Ri defined by the normalized number of broken bonds along direction *i*. All moments are extracted from the XMCD data obtained for stripes below the 2D coalescence.

→bcc transition the magnetostatic anisotropy, which favors in-plane anisotropy, is clearly dominating over the magnetocrystalline anisotropy.

In order to describe more quantitatively the magnetic anisotropy for the Fe stripes (0–1.5 ML's) we will focus specifically on this morphology. As described by Shen *et al.*[14] the first stage of growth of the Fe nanostructures is defined as elongated stripes 10–20 nm in the *x* direction, parallel to the steps, and 2–3 nm along the *y* direction, perpendicular to the steps. Thus along the *y* direction, a section with 10–15 atoms is obtained almost up to an equivalent thickness of 0.8 ML. During the first equivalent monolayer growth (0–1 ML) of Fe/Cu(111)-vic 1.2° this in-plane morphology undergoes only small changes, whereas along the growth direction *z* the single atomic layer Fe is progressively completed by the second layer. In this early stage of growth, the iron stripes show a strong in-plane anisotropy along $[1\bar{1}0]$ arising from the high aspect ratio. We should thus be able to describe the three orbital magnetic moments and their evolution up to the 2D coalescence by a simple model assuming a surface and a volume term for M_L^i. The related magnetocrystalline anisotropy will thus be connected to the difference of the surface to bulk ratio along both in-plane directions *X* and *Y*. In Fig. 3 we plot the M_L^i values obtained for different nanostructures below 1-ML Fe/Cu(111) as a function of the ratio R_i, where R_i represents the number of broken bonds over the total number of atoms along the *i* direction $(i=x, y, z)$. The linear dependence shows clearly that independently from the direction *i* the orbital magnetic moment M_L^i is defined by a ''volume'' iron fcc term of $0.035\mu_B$/atom and a ''surface'' term of $0.125\mu_B$/atom.

Moreover, the evolution of the differences ΔM_L (Fig. 4) shows that the magnetocrystalline anisotropy, proportional to $\Delta M_L=M_L^z-M_L^x$, before the 2D coalescence, decreases strongly whereas in the plane the differences $\Delta M_L=M_L^y-M_L^x$ keeps constant. This is related to the double layer growth in the out of plane direction *z*, whereas only a slight enlargement of the stripes is expected in the plane up to 1 ML. For the $3d$ elements where the ground-state spin-orbit coupling ξ is small compared to the crystal field and to the exchange interaction E_{ex} the MAE can be expressed by the

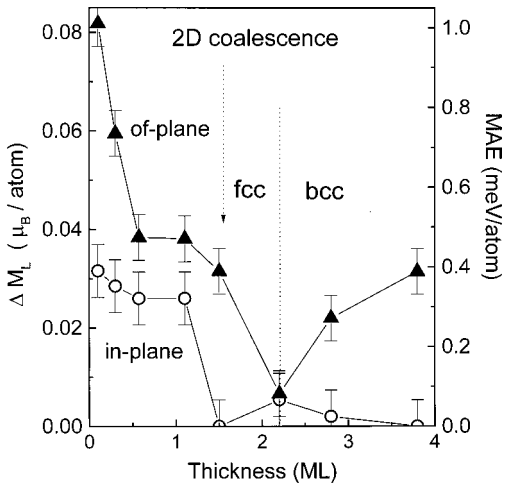

FIG. 4. Evolution of two orbital moment anisotropies ΔM_L (left axis) and calculated MAE's (right axis) with the thickness: The difference between the out-of-plane and the in-plane magnetic orbital moments $\Delta M_L^{\text{of-plane}}=(M_L^Z-M_L^X)$ is plotted for the out-of-plane magnetic anisotropy (filled triangles) and compared to the in-plane magnetic orbital moment anisotropies (open circles) given by $\Delta M_L^{\text{in-plane}}=(M_L^Y-M_L^X)$. The vertical dotted line at 2.3-ML thickness define the fcc→bcc phase transition.

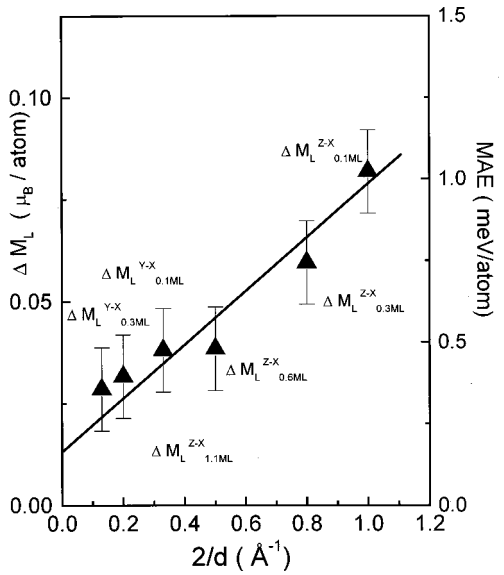

FIG. 5. Evolution of the orbital magnetic moment anisotropies $\Delta M_L=(M_L^i-M_L^X)$ (left axis) and calculated MAE's (right axis) as a function of the inverse thickness of the iron stripes $(2/d)$ along direction i. The plotted ΔM_L^i values are obtained with respect to the X axis, assuming that the stripes are infinite along the X direction.

following expression given by Bruno[21,22] linking the orbital anisotropy ΔM_L to the anisotropy energy:

$$\text{MAE}=-\frac{\xi}{4\mu_B}[(M_L^Z-M_L^X)^{\uparrow}-(M_L^Z-M_L^X)^{\downarrow}]+\frac{3\xi^2}{2E_{\text{ex}}\mu_B}(7M_T^Z-7M_T^X).$$

The MAE is obtained neglecting the majority spins and introducing a spin-orbit coupling constant $\xi=50$ meV.[21] We shall also neglect the dipolar spin magnetic-moment anisotropy energy which is quadratic in ξ. This approximation is confirmed by our measurements on the Fe nanostructures studied in this work where $M_S^{\text{eff}}(\theta)$ show no angular dependence inside the error bars related to low dipolar magnetic moments M_T.

In this framework a large out of plane MAE value of 1 meV/atom is found for the 1-ML-height Fe stripes [0.15-ML Fe/Cu(111)] in the Z direction decreasing to less to 0.4 meV/atom for the double layer stripes (0.8-ML Fe). The out-of-plane anisotropy vanishes completely at the phase transition (2.3 ML's). The large in-plane anisotropy (0.4 meV/atom) related to the constant aspect ratio in the plane decreases down to 0 at the 2D coalescence confirming the role of shape of the iron stripes. As compared to theoretical work the 1-meV/atom MAE of the 1-ML situation is close to the free-standing monolayer (111)-oriented fcc iron value found by Bruno and Renard[22] in the range 0.6–1.2 meV/atom.

Assuming that at 0.1 ML the stripes are infinite in the x direction parallel to the steps, the two previous magnetic anisotropies defined using XMCD ($M_L^i-M_L^x$, $i=z$ or y) can be considered as a combination of a surface term and a volume term. Thus in order to verify the validity of the linear evolution of the effective magnetic anisotropy as a function of $1/d$ and including the in and out of plane anisotropy on the same footing we plot in Fig. 5 the effective magnetic anisotropy energy extracted from Bruno's formula[21] and stemming from all our data points for fcc Fe below 1-ML Fe/Cu(111). The linear evolution scales with $1/d$ in the restricted thickness range considered. This can thus be described by an effective anisotropy energy per atom:

$$\text{MAE}_{\text{eff}}=\text{MAE}_V+\frac{2}{d}\text{MAE}_S. \tag{3}$$

The straight-line fit shows that all directions can be coherently described by a broken bond effect and that we can extract a direction independent magnetocrystalline surface anisotropy energy $\text{MAE}_S=1$ meV/atom and a volume anisotropy energy of $\text{MAE}_V=0.1$ meV/atom. This shows that surface MAE is ten times larger than the bulk contribution. Recent calculations[25] show that the surface contribution to the MAE turns out to be an order of magnitude higher (0.1 meV/atom) than the volume contribution (0.01 meV/atom). Our XMCD measured surface versus bulk MAE's are in perfect agreement with this calculations but lead to one order of magnitude larger numerical values. This has recently been explained by the fact that XMCD measurements of the MAE differ fundamentally from those obtained by the macroscopic low-energy techniques (SMOKE, ferromagnetic resonance).[26]

As compared with previously published data of MAE for fcc $Fe_{65}Ni_{35}$ nanostructures on Cu(111)-vic 1.2° the present values scales by a factor of 2 in the thickness range between 0.7 and 1.5 ML's. But unlike with the previous data, the in-plane anisotropy is present on the oriented Fe stripes below the coverage of 0.5 ML whereas the $Fe_{65}Ni_{35}$ islands do

not show any in-plane anisotropy in this range. We attribute the absence of anisotropy in the plane to the in-plane isotropic circular shape of the $Fe_{65}Ni_{35}$ nanostructures. This is one further indication that the in-plane uniaxial morphology is mandatory for in-plane MAE in the ultrathin film limit.

III. CONCLUSION

Epitaxially grown Fe stripes show strong in-plane and out-of-plane magnetic anisotropies related to the growth on a Cu(111) vicinal surface. A huge increase of M_L is observed depending on the direction of saturation of the applied field. The correlation between M_L^i and the number of Fe atoms leads to the conclusion that the enhancement of the orbital moment along one direction is connected to the number of broken bonds along this direction. A ratio of 4 is obtained between surface and bulk orbital moments. According to our model the influence of the copper interface is absent both in the direction dependence of M_L and in the anisotropy of the moments. This will induce an isotropic electronic structure of the pseudomorphic Fe/Cu interface.

One monolayer thick iron stripes show a 1 meV/at MAE whereas the value in the plane is 0.4 meV/atom for the Fe stripes below 1-ML Fe. This is related to the size of the in-plane stripes compared to the monolayer-high stripes in the first stage of the growth. The orbital magnetic moment show a directionally independent correlation with the number of broken bonds. We determine a volume and a surface contribution of the orbital moment and of the MAE. The surface contribution is shown to be one order of magnitude larger than the volume MAE of fcc Fe.

ACKNOWLEDGMENTS

The authors thank K. Larsson, B. Muller, and J. G. Faullumel for technical help during the XMCD experiments. This work was supported by the Center National de la Recherche Scientifique (CNRS-ULTIMATECH program).

*Corresponding author. Fax: (+33) 3 88 10 72 48. Email address: christine.boeglin@ipcms.u-strasbg.fr

[1] W. Weber *et al.*, Phys. Rev. Lett. **76**, 1940 (1996).
[2] H. A. Dürr, G. van der Laan, J. Vogel, G. Panaccione, N. B. Brookes, E. Dudzik, and R. McGrath, Phys. Rev. B **58**, R11 853 (1998).
[3] S. Cherifi, C. Boeglin, S. Stanescu, J. P. Deville, C. Mocuta, P. Ohresser, and N. B. Brookes, Phys. Rev. B **64**, 184405 (2001).
[4] P. Ohresser, G. Ghiringhelli, O. Tjernberg, N. B. Brookes, and M. Finazzi, Phys. Rev. B **62**, 5803 (2000).
[5] H. A. Dürr, S. S. Dhesi, E. Dudzik, D. Knabben, G. Van der Laan, J. B. Goedkoop, and F. U. Hillebrecht, Phys. Rev. B **59**, R701 (1999).
[6] T. Koide, H. Miyauchi, J. Okamoto, T. Shidara, A. Fujimori, H. Fukutani, K. Amemiya, H. Takeshita, S. Yuasa, T. Katayama, and Y. Suzuki, Phys. Rev. Lett. **87**, 257201 (2001).
[7] J. Chen and J. L. Erskine, Phys. Rev. Lett. **68**, 1212 (1992).
[8] A. Berger, U. Linke, and H. P. Oepen, Phys. Rev. Lett. **68**, 839 (1992).
[9] W. Weber *et al.*, Phys. Rev. Lett. **76**, 1940 (1996).
[10] R. K. Kawakami, E. J. Escorcia-Aparicio, and Z. Q. Qiu, Phys. Rev. Lett. **77**, 2570 (1996).
[11] J. Escorcia-Aparicio, H. J. Choi, W. L. Ling, R. K. Kawakami, and Z. Q. Qiu, Phys. Rev. Lett. **81**, 2144 (1998).
[12] R. A. Hyman, A. Zangwill, and M. D. Stiles, Phys. Rev. B **58**, 9276 (1998).
[13] J. Dorantes-Davila and G. Pastor, Phys. Rev. Lett. **81**, 208 (1998).
[14] J. Shen, R. Skomski, M. Klaua, H. Jenniches, S. Sundar Manoharan, and J. Kirschner, Phys. Rev. B **56**, 2340 (1997).
[15] J. Shen, M. Klaua, P. Ohresser, H. Jenniches, J. Bartel, Ch. V. Mohan, and J. Kirschner, Phys. Rev. B **56**, 11 134 (1997).
[16] B. T. Thole, P. Carra, F. Sette, and G. van der Laan, Phys. Rev. Lett. **68**, 1943 (1992).
[17] P. Carra, B. T. Thole, M. Altarelli, and X. Wang, Phys. Rev. Lett. **70**, 694 (1993).
[18] J. Stöhr, J. Magn. Magn. Mater. **200**, 470 (1999).
[19] J. Stöhr and H. König, Phys. Rev. Lett. **75**, 3748 (1995); D. Weller, J. Stöhr, R. Nakajima, A. Carl, M. G. Samant, C. Chappert, R. Mégy, P. Beauvillain, P. Veillet, and G. A. Held, *ibid.* **75**, 3752 (1995).
[20] R. Nakajima, J. Stöhr, and Y. U. Idzerda, Phys. Rev. B **59**, 6421 (1999).
[21] P. Bruno, Phys. Rev. B **39**, 865 (1989).
[22] P. Bruno and J. P. Renard, Appl. Phys. A: Solids Surf. **A49**, 499 (1989).
[23] H. A. Dürr, G. Y. Guo, G. van der Laan, J. Lee, G. Lauhoff, and J. A. Bland, Science **277**, 213 (1997).
[24] G. van der Laan, J. Phys.: Condens. Matter **10**, 3239 (1998).
[25] A. B. Shick, Yu. N. Gornostyrev, and A. J. Freeman, Phys. Rev. B **60**, 3029 (1999).
[26] S. S. Dhesi, G. van der Laan, E. Dudzik, and A. B. Shick, Phys. Rev. Lett. **87**, 067201 (2001).